Spiral spin-liquid and the emergence of a vortex-like state in $MnSc_2S_4$

Shang Gao[1,2], Oksana Zaharko[1]*, Vladimir Tsurkan[3,4], Yixi Su[5], Jonathan S. White[1], Gregory S. Tucker[1,6], Bertrand Roessli[1], Frederic Bourdarot[7], Romain Sibille[1,8], Dmitry Chernyshov[9], Tom Fennell[1], Alois Loidl[3] and Christian Rüegg[1,2]

Spirals and helices are common motifs of long-range order in magnetic solids, and they may also be organized into more complex emergent structures such as magnetic skyrmions and vortices. A new type of spiral state, the spiral spin-liquid, in which spins fluctuate collectively as spirals, has recently been predicted to exist. Here, using neutron scattering techniques, we experimentally prove the existence of a spiral spin-liquid in $MnSc_2S_4$ by directly observing the 'spiral surface'—a continuous surface of spiral propagation vectors in reciprocal space. We elucidate the multi-step ordering behaviour of the spiral spin-liquid, and discover a vortex-like triple-q phase on application of a magnetic field. Our results prove the effectiveness of the J_1–J_2 Hamiltonian on the diamond lattice as a model for the spiral spin-liquid state in $MnSc_2S_4$, and also demonstrate a new way to realize a magnetic vortex lattice through frustrated interactions.

Magnetic frustration, where magnetic moments (spins) are coupled through competing interactions that cannot be simultaneously satisfied[1], usually leads to highly cooperative spin fluctuations[2,3] and unconventional long-range magnetic order[4,5]. An archetypal ordering in the presence of frustration is the spin spiral. Competing interactions and spiral orders give rise to many phenomena in magnetism, including the multitudinous magnetic phases of rare earth metals[6], domains with multiferroic properties[7,8], and topologically non-trivial structures such as the emergent skyrmion lattice[9–12].

Recently, a new spiral state—a spiral spin-liquid in which the ground states are a massively degenerate set of coplanar spin spirals—was predicted to exist in the J_1–J_2 model on the diamond lattice (see Fig. 1a)[13–15]. Although the diamond lattice is bipartite, and therefore unfrustrated at the near-neighbour (J_1) level, the second-neighbour coupling (J_2) can generate strong competition. For classical spins, mean-field calculations show that when $|J_2/J_1| > 0.125$ the spiral spin-liquid appears, and that it is signified by an unusual continuous surface of propagation vectors $\boldsymbol{q}$ in reciprocal space (see Fig. 1b for the spiral surface of $|J_2/J_1| = 0.85$). At finite temperature, thermal fluctuations might select some specific $\boldsymbol{q}$-vectors on the spiral surface[13], resulting in an order-by-disorder transition[16,17].

Until now, several series of A-site spinels, in which the magnetic A ions form a diamond lattice, have been investigated, including: the cobaltates Co_3O_4 and $CoRh_2O_4$ (ref. 18); the aluminates MAl_2O_4 with M = Fe, Co, Mn[19–23]; and the scandium thiospinels MSc_2S_4 with M = Fe, Mn[24]. For the spinels with Fe^{2+} at the A-site, the e_g orbital angular momentum of Fe^{2+} is active, making the pure spin J_1–J_2 model inadequate[25]. Among the other compounds, $CoAl_2O_4$ and $MnSc_2S_4$ manifest the strongest frustration. For $CoAl_2O_4$, the ratio of $|J_2/J_1|$ has been identified as 0.109 (ref. 21), which is near, but still lower than, the 0.125 threshold for the spiral spin-liquid state. Many experimental studies of $MnSc_2S_4$ (refs 24,26–30) suggest its relevance to the spiral spin-liquid, but the spiral surface has not been observed.

In this article, we present the results of extensive experimental studies of high-quality single crystals of $MnSc_2S_4$ by neutron scattering. Our diffuse scattering data uncovers the spiral surface, providing direct evidence for the proposed spiral spin-liquid state. The spiral spin-liquid enters a helical long-range ordered state through a multi-step ordering process, which we suggest is due to dipolar and third-neighbour (J_3) perturbations, which we quantify. Finally, by applying a magnetic field, an emergent triple-$\boldsymbol{q}$ phase is discovered. The $\boldsymbol{q}$ combination rule of this field-induced phase is similar to that observed in the skyrmion lattice[9,10], which suggests A-site spinels are new candidate systems to realize the atomic-sized vortex lattice states[31–36].

Neutron diffuse scattering measures the reciprocal space distribution of the quasi-static spin correlations and provides direct information on the ground state degeneracy in frustrated systems[37,38]. Figure 1c presents our diffuse scattering results for the (HK0) plane of $MnSc_2S_4$, measured at 2.9 K. Strong intensities are observed near the Brillouin zone boundaries, forming a squared-ring pattern. This pattern, with its large span and non-ellipsoidal form in reciprocal space, is very different from those observed in less-frustrated systems such as $CoAl_2O_4$ (refs 21,22), where intensities centre closely around magnetic Bragg points that characterize incipient order.

[1]Laboratory for Neutron Scattering and Imaging, Paul Scherrer Institut, CH-5232 Villigen PSI, Switzerland. [2]Department of Quantum Matter Physics, University of Geneva, CH-1211 Geneva, Switzerland. [3]Experimental Physics V, University of Augsburg, D-86135 Augsburg, Germany. [4]Institute of Applied Physics, Academy of Sciences of Moldova, MD-2028 Chisinau, Republic of Moldova. [5]Jülich Center for Neutron Science JCNS-MLZ, Forshungszentrum Jülich GmbH, Outstation at MLZ, D-85747 Garching, Germany. [6]Laboratory for Quantum Magnetism, École Polytechnique Fédérale de Lausanne, CH-1015 Lausanne, Switzerland. [7]CEA et Université Grenoble Alpes, INAC-MEM-MDN, F-38000 Grenoble, France. [8]Laboratory for Scientific Developments and Novel Materials, Paul Scherrer Institut, CH-5232 Villigen PSI, Switzerland. [9]Swiss-Norwegian Beamlines at the European Synchrotron Radiation Facility, F-38000 Grenoble, France. *e-mail: oksana.zaharko@psi.ch

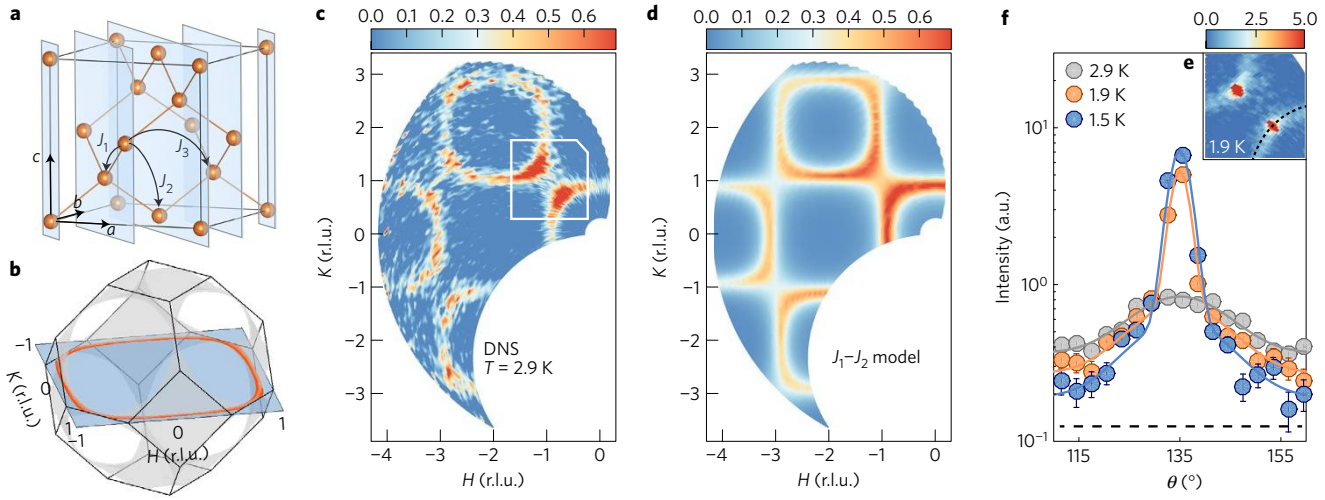

Figure 1 | Spiral spin-liquid. a, Diamond lattice of Mn^{2+} ions in $MnSc_2S_4$, (110) planes are shaded blue. **b**, Spiral surface (grey) predicted by mean-field theory for the J_1–J_2 model with the ratio $|J_2/J_1| = 0.85$. The red ring emphasizes a cut within the (*HK*0) plane (blue). **c**, Diffuse scattering intensities in the (*HK*0) plane measured at 2.9 K. The white square outlines the area shown in **e**. **d**, Monte Carlo simulations for spin correlations in the (*HK*0) plane using the J_1–J_2 model with the ratio $|J_2/J_1| = 0.85$ and $T/|J_1| = 0.55$. **e**, Diffuse scattering intensities around (110) (contour outlined in **c**) measured at 1.9 K, showing the coexistence of Bragg peaks and the diffuse signal. The dashed arc describes the path for the 1D cut presented in **f**, where the polar angle θ is used as the *x* axis. **f**, Comparison of the 1D cut at $T = 2.9$, 1.9 and 1.5 K, showing the diffuse signal extending down to the base temperature of 1.5 K. Integrations are performed in the polar coordinate system with a fixed radius of 1.06 and an integration width of 0.3. The solid lines are fits to a constant and a broad Gaussian function to model the diffuse scattering, and to an additional Gaussian function for Bragg scattering at $T = 1.9$ and 1.5 K. The horizontal dashed line indicates the background level estimated from an integration with a smaller radius of 0.8. Error bars represent standard deviations.

According to mean-field calculations[13], a larger ratio of $|J_2/J_1|$ causes increased frustration and is accompanied by the expansion of the spiral surface in reciprocal space, expanding the ring in the (*HK*0) plane towards the Brillouin zone boundary. Thus, the observed squared-ring feature affirms that $MnSc_2S_4$ is strongly frustrated.

Monte Carlo simulations of the J_1–J_2 model on a $10 \times 10 \times 10$ superlattice can be directly compared with the experiment. The simulated neutron scattering pattern for the ratio $|J_2/J_1| = 0.85$ and $T/|J_1| = 0.55$ is shown in Fig. 1d. In ref. 13, this ratio of $|J_2/J_1|$ was shown to be a highly frustrated case of the Hamiltonian, with the spiral spin-liquid as its ground state. Thus, the experimentally observed diffuse scattering directly proves the existence of the spiral surface and the spiral spin-liquid state in $MnSc_2S_4$.

Previous studies revealed a transition into a commensurate long-range ordered state with $\boldsymbol{q} = (0.75\ 0.75\ 0)$ at $T \sim 2.3$ K (refs 24,26). Figure 1e shows the data at 1.9 K for the region around $(-1\ 1\ 0)$. Two strong magnetic Bragg peaks have appeared at $(-0.75\ 0.75\ 0)$ and $(-1.25\ 1.25\ 0)$, but a trace of the spiral surface is still discernible below the long-range ordering transition. One-dimensional (1D) cuts along the arc of the spiral surface at different temperatures are compared in Fig. 1f, revealing the coexistence of long-range and short-range correlations down to 1.5 K (the base temperature of the diffuse scattering experiment). Such a coexistence signals the presence of strong fluctuations in the ordered phase and calls for a detailed study of the ordering behaviour in $MnSc_2S_4$.

Using single-crystal neutron diffraction, which is a direct probe of the long-range ordered state, we investigated the ordering to lower temperatures. Figure 2a–c presents scans along the $[1\bar{1}0]$ direction for the (0.75 0.75 0) peak at $T = 1.68$, 1.60, 1.44 K. In the region $1.64 > T > 1.46$ K, an incommensurate (IC) phase with the propagation vector $\boldsymbol{q}' = (0.75 \pm 0.02\ 0.75 \mp 0.02\ 0)$ was discovered, suggesting that the ordering of the spiral spin-liquid involves a multi-step process.

This multi-step character is also evident in our spherical neutron polarimetry (SNP) experiments[39]. Figure 2d plots the temperature dependence of the P_{yy} polarization element of the (0.75 0.75 0) peak, which describes the difference of the magnetic structure factors *M* along $\hat{y}/\hat{z}$ directions ($\hat{x}$ along $[\bar{1}\bar{1}0]$, $\hat{y}$ along [001], and $\hat{z}$ along $[\bar{1}10]$ for (*HHL*) plane horizontal): $P_{yy} = (M_y M_y^* - M_z M_z^*)/(M_y M_y^* + M_z M_z^*)$. The evolution of P_{yy} from -0.8 to -0.1 with decreasing T unambiguously reveals that the two commensurate phases for $T > 1.64$ K and $T < 1.46$ K possess different magnetic structures, even though their $\boldsymbol{q}$-vectors are exactly the same.

To determine the magnetic structures, complete sets of magnetic Bragg peak intensities were collected by neutron diffraction at $T = 1.38$ and 1.70 K and compared with theoretical models. The previously proposed cycloidal structure[26] failed to fit either data set. Instead, at 1.38 K a helical structure (Fig. 3a, top), and at 1.70 K a sinusoidally modulated collinear structure (Fig. 3a, bottom) were found to successfully reproduce the data sets. The transition from the collinear structure to the helical structure occurs through the incommensurate phase, whose narrow temperature window is consistent with the continuous growth of the SNP P_{yy} element for $1.64 > T > 1.46$ K.

According to previous theoretical studies[13,14], the inclusion of an antiferromagnetic J_3 perturbation in the J_1–J_2 model selects the $\boldsymbol{q}$ position for the spiral but leaves the spiral plane undetermined; whether the ground state is cycloidal or helical depends on further anisotropic perturbations. Here, the observed helical structure provides strong evidence for the effect of dipolar interactions, which have been shown to favour the helical structure over the cycloidal structure[14]. Previous calculations reveal that a value of $J_3 \sim -0.04$ K brings $\boldsymbol{q}$ to (0.75 0.75 0) (refs 13,14), and the dipolar interaction is ~0.026 K for nearest neighbours. However, our mean-field calculations reveal that long-range order at $\boldsymbol{q} = (0.75\ 0.75\ 0)$ occurs even in the case where J_3 equals zero and only the dipolar perturbation exists. Dipolar interactions might also contribute to the appearance of the collinear phase. By decomposing the $\boldsymbol{q} = (0.75\ 0.75\ 0)$ helicoid into two sinusoidally modulated collinear structures with spins along the $[1\bar{1}0]$ and [001] directions, we find that the dipolar interactions favour the $[1\bar{1}0]$ direction by an energy difference of 0.003 K per spin. This in-plane anisotropy stabilizes the helicoid in-plane component and helps the development of the observed collinear phase[8,40]. We note that all these perturbations

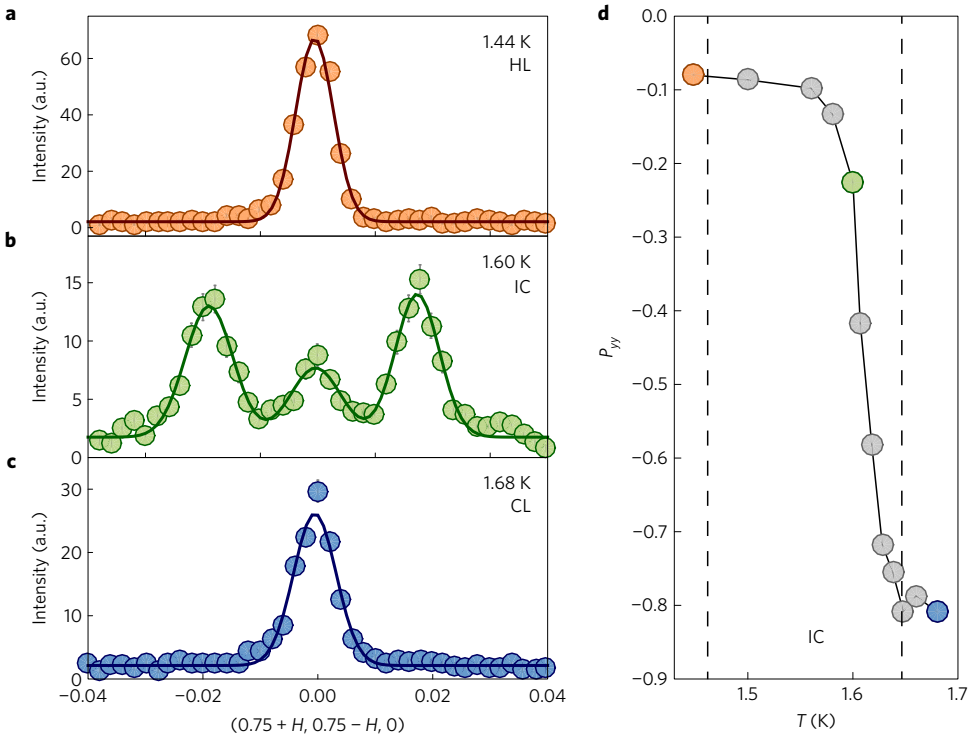

Figure 2 | Multi-step ordering towards the helical ground state. a–c, Neutron diffraction data along the [1$\bar{1}$0] direction for the (0.75 0.75 0) reflection measured at 1.44, 1.60, and 1.68 K during cooling. HL, IC, and CL represent the helical, incommensurate and sinusoidally modulated collinear phases, respectively. **d**, Temperature dependence of the SNP element P_{yy} measured with the (*HHL*) plane horizontal. Orange, green, and blue points correspond to $T = 1.44, 1.60$, and 1.68 K, respectively. Error bars represent standard deviations.

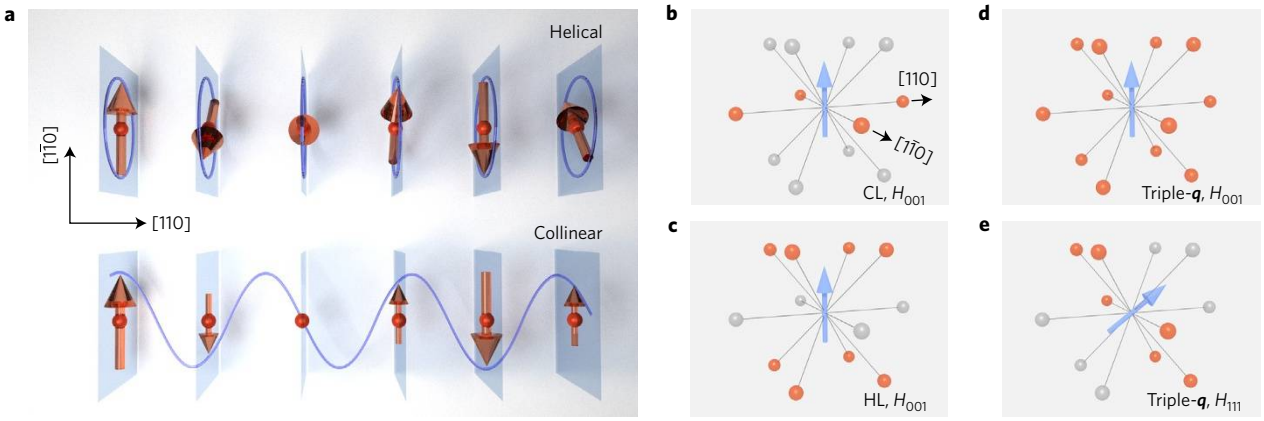

Figure 3 | Spin structures and their magnetic field response. a, The helical structure (top) and the sinusoidally modulated collinear structure (bottom) refined from 1.38 and 1.70 K data sets with $R_{f2} = 0.14$ and 0.17, respectively. Blue shaded planes are perpendicular to the propagation vector (for example, (110) planes for $\boldsymbol{q} = (0.75\ 0.75\ 0)$, which are also shown in the crystal structure of Fig. 1a); over these planes the ordered moments have the same size and orientation. For the helical structure, the moment is refined to be $5.27(23)\mu_B$ (where μ_B is the Bohr magneton). For the collinear structure, the moment is sinusoidally modulated from 0 to $4.77(20)\mu_B$. **b–e**, Intensity distribution for the 12 arms of the ⟨0.75 0.75 0⟩ star under magnetic field. They are extracted from refinements of neutron diffraction data sets. Orange spheres indicate arms with nearly equal intensities; grey spheres indicate arms with zero intensities; and blue arrows indicate the field directions. **b**, Distribution in the collinear phase measured at $T = 1.80$ K under a [001] magnetic field of 3.5 T. **c**, Expected distribution in the helical phase under a [001] magnetic field, experimentally confirming the disappearance of the arms in the (001) plane are for H below ~3 T. **d**, Distribution in the triple-$\boldsymbol{q}$ phase measured at $T = 1.30$ K under a 3.5 T magnetic field along [001]. **e**, Distribution in the triple-$\boldsymbol{q}$ phase measured at $T = 1.60$ K under a 3.5 T magnetic field along [111].

are small compared to J_1 and J_2, such that the spiral spin-liquid we observed appears to be fairly ideal, as evidenced by the close agreement between J_1–J_2 theory and experiment in Fig. 1c,d.

The established collinear and helical phases are both single-$\boldsymbol{q}$ structures, meaning that the 12 arms of the ⟨0.75 0.75 0⟩ star form independent magnetic domains. Figure 3b,c summarizes the response of all the 12 arms for the collinear and helical phases when we applied a magnetic field along the [001] direction. As is discussed in the Supplementary Information, the observed intensity distributions are consistent with the anisotropic susceptibility effect expected for magnetic domains and confirm the single-$\boldsymbol{q}$ character of the collinear and helical phases.

However, after cooling from the collinear phase in a field of 3.5 T, refinements of the neutron diffraction data sets reveal that, although

the single-arm structure stays the same, the previously suppressed arms reappear with all the 12 arms having about the same intensities. This intensity redistribution, which is summarized in Fig. 3d, is contradictory to the domain effect expected for a single-$\boldsymbol{q}$ structure, and evidences the emergence of a field-induced multi-$\boldsymbol{q}$ phase. By studying the H and T dependence of the intensity of the (0.75 0.75 0) Bragg peak (typical scans are shown in Fig. 4a,b), the extent of this multi-$\boldsymbol{q}$ phase is mapped out in Fig. 4c.

We propose the field-induced phase to be a triple-$\boldsymbol{q}$ state with:

$$\boldsymbol{M}(\boldsymbol{r}) = \sum_{j=1}^{3} (\boldsymbol{m}_j e^{i(\boldsymbol{q}_j \cdot \boldsymbol{r} + \phi_j)} + \text{c.c.}) \quad (1)$$

where the three coplanar $\boldsymbol{q}_j$ satisfy $\sum_{j=1}^{3} \boldsymbol{q}_j = 0$ (for example, $\boldsymbol{q}_1 = (0.75\ 0.75\ 0)$, $\boldsymbol{q}_2 = (0\ \overline{0.75}\ 0.75)$, and $\boldsymbol{q}_3 = (\overline{0.75}\ 0\ \overline{0.75})$), similar to that observed in the skyrmion lattice[10]; $\boldsymbol{m}_j$ is the real basis vector perpendicular to $\boldsymbol{q}_j$; ϕ_j describes an additional phase factor; and c.c. is the complex conjugate. Four triple-$\boldsymbol{q}$ domains formed in this way are symmetrically equivalent under the [001] magnetic field, which explains the equal intensity distribution shown in Fig. 3d. In contrast, in Fig. 3e we plot the distribution measured under a 3.5 T magnetic field along the [111] direction. This [111] field breaks the symmetry; therefore, only one triple-$\boldsymbol{q}$ domain with arms perpendicular to H can be observed.

Neutron diffraction is not sensitive to the phase factor ϕ_j. In the Supplementary Information, we present two possible structures that preserve the C_3 symmetry along the [111] direction together with the expected structures with a shorter $\boldsymbol{q} = (0.25\ 0.25\ 0)$ that might be realized in less-frustrated A-site spinels[13]. In these structures, spin components in the (111) plane exhibit a winding behaviour around the C_3 axis, resulting in a vortex state similar to that predicted in frustrated antiferromagnets[31–33]. Considering that the winding feature persists regardless of the choice of ϕ_j, our experiments reveal the A-site spinels to be a new system in which to realize a vortex lattice.

Compared with the well-established skyrmion lattices[9], the observed vortex lattice is distinctive in its real basis vectors $\boldsymbol{m}_j$, which should be complex for the skyrmion lattices. As is shown in the Supplementary Information, this difference of the basis vector affects the spin ordering perpendicular to the plane expanded by the three basis $\boldsymbol{q}$-vectors and gives rise to different topologies for these two states. On the other aspect, it is important to note that the driving forces of the spin twisting in these two lattices are very different: in known skyrmion lattices, it originates from the relativistic Dzyaloshinskii–Moriya interaction[9,10]; while in the $MnSc_2S_4$ vortex lattice, it is a pure frustration effect[32,33], which leads to its much smaller vortex size in contrast to the known skyrmions[9–12].

In theory, thermal fluctuations select an ordered state with $\boldsymbol{q} \sim (001)$ for the spiral spin-liquid by an order-by-disorder mechanism[13]. The multi-step ordering process and wavevector we have observed show clearly that $MnSc_2S_4$ does not support an order-by-disorder transition. Our studies show that, for the prospect of realizing an order-by-disorder transition, it is crucial to identify materials with reduced perturbations from the dipolar and further-neighbour exchange interactions. However, it is clear that fluctuations play an essential, but not understood, role in $MnSc_2S_4$. The collinear phase retains considerable spin fluctuations, as manifested in the amplitude modulation of its ordered moments. We speculate that the progressive suppression of these fluctuations on cooling could set up a temperature-dependent dipolar interaction whose changing competition with the exchange interactions could be at the origin of the incommensurate phase. On the other hand, the search for spiral spin-liquids and order-by-disorder transition should not be restricted to the A-site spinels, or even to the diamond lattice. The primary constituent to realize spiral spin-liquids is the frustrated J_1–J_2 model, which can be constructed for most bipartite

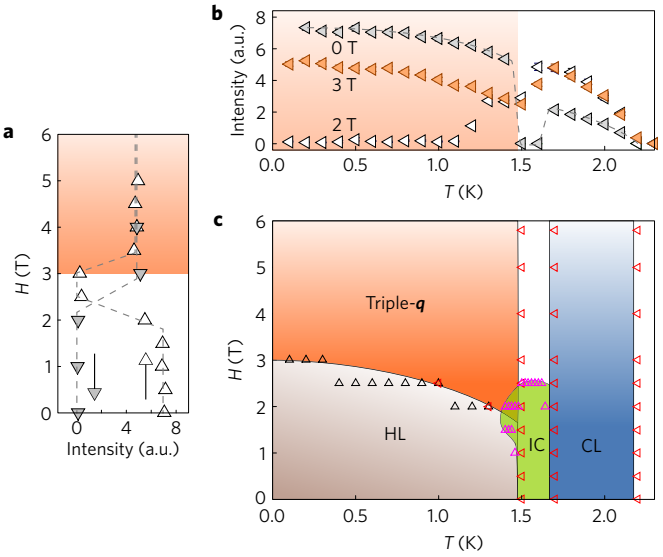

Figure 4 | Phase diagram of $MnSc_2S_4$ under a magnetic field along the [001] direction. a, Field dependence of the intensity of the (0.75 0.75 0) reflection measured at $T = 0.1$ K. Up-pointing open (down-pointing filled) triangles belong to the measurements with increasing (decreasing) field. **b**, Temperature dependence of the neutron diffraction intensity of the (0.75 0.75 0) reflection measured under different magnetic fields. **c**, Phase diagram from neutron diffraction experiments. Up-pointing (left-pointing) triangles mark the transition positions extracted from the measurements with increasing field (decreasing temperature). HL, CL, and IC represent the helical, sinusoidally modulated collinear, and incommensurate phases, respectively. The IC phase disappears under field cooling. Error bars in **a**,**b** represent standard deviations and are smaller than the symbol size.

lattices. One recent example is the honeycomb lattice, where a two-dimensional analogue of the spiral spin-liquid state and a subsequent order-by-disorder transition have been predicted[41].

In summary, by neutron diffraction and diffuse scattering, we confirm the existence of a spiral spin-liquid in $MnSc_2S_4$, which exhibits the most frustrated ratio of $|J_2/J_1| = 0.85$ in the known A-site spinels. At lower temperature, a multi-step ordering process of the spiral spin-liquid is observed, reflecting the significance of dipolar interactions in $MnSc_2S_4$. Under magnetic field, an emergent vortex-like triple-$\boldsymbol{q}$ phase is discovered, which establishes the A-site spinel as a promising system to realize vortex lattice states.

References

1. Balents, L. Spin liquids in frustrated magnets. *Nature* **464,** 199–208 (2010).
2. Bramwell, S. T. & Gingras, M. J. P. Spin ice state in frustrated magnetic pyrochlore materials. *Science* **294,** 1495–1501 (2001).
3. Henley, C. L. The Coulomb phase in frustrated systems. *Annu. Rev. Condens. Matter Phys.* **1,** 179–210 (2010).
4. Reimers, J. N., Berlinsky, A. J. & Shi, A. C. Mean-field approach to magnetic ordering in highly frustrated pyrochlores. *Phys. Rev. B* **43,** 865–878 (1991).
5. Tchernyshyov, O., Moessner, R. & Sondhi, S. L. Order by distortion and string modes in pyrochlore antiferromagnets. *Phys. Rev. Lett.* **88,** 067203 (2002).
6. Jensen, J. & Mackintosh, A. R. *Rare Earth Magnetism* (Clarendon, 1991).
7. Cheong, S.-W. & Mostovoy, M. Multiferroics: a magnetic twist for ferroelectricity. *Nat. Mater.* **6,** 13–20 (2007).

8. Mostovoy, M. Ferroelectricity in spiral magnets. *Phys. Rev. Lett.* **96,** 067601 (2006).
9. Nagaosa, N. & Tokura, Y. Topological properties and dynamics of magnetic skyrmions. *Nat. Nanotech.* **8,** 899–911 (2013).
10. Mühlbauer, S. *et al*. Skyrmion lattice in a chiral magnet. *Science* **323,** 915–919 (2009).
11. Kézsmárki, I. *et al*. Néel-type skyrmion lattice with confined orientation in the polar magnetic semiconductor GaV_4S_8. *Nat. Mater.* **14,** 1116–1122 (2015).
12. Tokunaga, Y. *et al*. A new class of chiral materials hosting magnetic skyrmions beyond room temperature. *Nat. Commun.* **6,** 7638 (2015).
13. Bergman, D., Alicea, J., Gull, E., Trebst, S. & Balents, L. Order-by-disorder and spiral spin-liquid in frustrated diamond-lattice antiferromagnets. *Nat. Phys.* **3,** 487–491 (2007).
14. Lee, S. B. & Balents, L. Theory of the ordered phase in *A*-site antiferromagnetic spinels. *Phys. Rev. B* **78,** 144417 (2008).
15. Savary, L. *et al*. Impurity effects in highly frustrated diamond-lattice antiferromagnets. *Phys. Rev. B* **84,** 064438 (2011).
16. Villain, J., Bidaux, R., Carton, J.-P. & Conte, R. Order as an effect of disorder. *J. Phys.* **41,** 1263–1272 (1980).
17. Henley, C. L. Ordering due to disorder in a frustrated vector antiferromagnet. *Phys. Rev. Lett.* **62,** 2056–2059 (1989).
18. Suzuki, T., Nagai, H., Nohara, M. & Takagi, H. Melting of antiferromagnetic ordering in spinel oxide $CoAl_2O_4$. *J. Phys. Condens. Matter* **19,** 145265 (2007).
19. Tristan, N. *et al*. Geometric frustration in the cubic spinels MAl_2O_4 (M = Co, Fe, and Mn). *Phys. Rev. B* **72,** 174404 (2005).
20. Krimmel, A., Mutka, H., Koza, M. M., Tsurkan, V. & Loidl, A. Spin excitations in frustrated *A*-site spinels investigated with inelastic neutron scattering. *Phys. Rev. B* **79,** 134406 (2009).
21. Zaharko, O. *et al*. Spin liquid in a single crystal of the frustrated diamond lattice antiferromagnet $CoAl_2O_4$. *Phys. Rev. B* **84,** 094403 (2011).
22. MacDougall, G. J. *et al*. Kinetically inhibited order in a diamond-lattice antiferromagnet. *Proc. Natl Acad. Sci. USA* **108,** 15693–15698 (2011).
23. Nair, H. S., Fu, Z., Voigt, J., Su, Y. X. & Brückel, Th. Approaching the true ground state of frustrated *A*-site spinels: a combined magnetization and polarized neutron scattering study. *Phys. Rev. B* **89,** 174431 (2014).
24. Fritsch, V. *et al*. Spin and orbital frustration in $MnSc_2S_4$ and $FeSc_2S_4$. *Phys. Rev. Lett.* **92,** 116401 (2004).
25. Chen, G., Balents, L. & Schnyder, A. P. Spin-orbital singlet and quantum critical point on the diamond lattice: $FeSc_2S_4$. *Phys. Rev. Lett.* **102,** 096406 (2009).
26. Krimmel, A. *et al*. Magnetic ordering and spin excitations in the frustrated magnet $MnSc_2S_4$. *Phys. Rev. B* **73,** 014413 (2006).
27. Mücksch, M. *et al*. Multi-step magnetic ordering in frustrated thiospinel $MnSc_2S_4$. *J. Phys. Condens. Matter* **19,** 145262 (2007).
28. Giri, S., Nakamura, H. & Kohara, T. Classical antiferromagnetism in $MnSc_2S_4$: a ^{45}Sc NMR study. *Phys. Rev. B* **72,** 132404 (2005).
29. Büttgen, N., Zymara, A., Kegler, C., Tsurkan, V. & Loidl, A. Spin and orbital frustration in $FeSc_2S_4$ probed by ^{45}Sc NMR. *Phys. Rev. B* **73,** 132409 (2006).
30. Kalvius, G. M. *et al*. A μSR magnetic study of frustrated $FeSc_2S_4$ and $MnSc_2S_4$. *Physica B* **378–380,** 592–593 (2006).
31. Batista, C. D., Lin, S.-Z., Hayami, S. & Kamiya, Y. Frustration and chiral orderings in correlated electron systems. *Rep. Prog. Phys.* **79,** 084504 (2016).
32. Kamiya, Y. & Batista, C. D. Magnetic vortex crystals in frustrated Mott insulator. *Phys. Rev. X* **4,** 011023 (2014).
33. Wang, Z., Kamiya, Y., Nevidomskyy, A. H. & Batista, C. D. Three-dimensional crystallization of vortex strings in frustrated quantum magnets. *Phys. Rev. Lett.* **115,** 107201 (2015).
34. Okubo, T., Chung, S. & Kawamura, H. Multiple-q states and the skyrmion lattice of the triangular-lattice Heisenberg antiferromagnet under magnetic fields. *Phys. Rev. Lett.* **108,** 017206 (2012).
35. Leonov, A. O. & Mostovoy, M. Multiply periodic states and isolated skyrmions in an anisotropic frustrated magnet. *Nat. Commun.* **6,** 8275 (2015).
36. Hayami, S., Lin, S.-Z. & Batista, C. D. Bubble and skyrmion crystals in frustrated magnets with easy-axis anisotropy. *Phys. Rev. B* **93,** 184413 (2016).
37. Reimers, J. N. Diffuse-magnetic-scattering calculations for frustrated antiferromagnets. *Phys. Rev. B* **46,** 193–202 (1992).
38. Fennell, T. *et al*. Magnetic Coulomb phase in the spin ice $Ho_2Ti_2O_7$. *Science* **326,** 415–417 (2009).
39. Brown, P. J. in *Neutron Scattering from Magnetic Materials* (ed. Chatterji, T.) (Elsevier, 2006).
40. Mochizuki, M. & Furukawa, N. Microscopic model and phase diagrams of the multiferroic perovskite manganites. *Phys. Rev. B* **80,** 134416 (2009).
41. Mulder, A., Ganesh, R., Capriotti, L. & Paramekanti, A. Spiral order by disorder and lattice nematic order in a frustrated Heisenberg antiferromagnet on the honeycomb lattice. *Phys. Rev. B* **81,** 214419 (2010).

Acknowledgements

We acknowledge helpful discussions with L. Balents, B. Normand, J. H. Chen, A. Scaramucci, A. Cervellino, S. Tóth, S. Ward and M. Ruminy. Our neutron scattering experiments were performed at the Swiss Spallation Neutron Source SINQ, Paul Scherrer Institut, Villigen, Switzerland, the Heinz Maier-Leibnitz Zentrum MLZ, Garching, Germany, and the Institut Laue-Langevin ILL, Grenoble, France. The magnetization measurements were carried out in the Laboratory for Scientific Developments and Novel Materials, Paul Scherrer Institut, Villigen, Switzerland. This work was supported by the Swiss National Science Foundation under Grants Nos 200021-140862 and 200020-162626, and the SCOPES project No. IZ73Z0-152734/1. Our work was additionally supported by the Swiss State Secretariat for Education, Research and Innovation (SERI) through a CRG-grant and via the Deutsche Forschungsgemeinschaft by the Transregional Collaborative Research Center TRR 80.

Author contributions

O.Z. and C.R. designed and supervised the project. V.T. prepared the single crystals. S.G. and O.Z. performed the experiments with Y.S. as the local contact for DNS, J.S.W. and G.S.T. for TASP, B.R. for MuPAD, F.B. for CRYOPAD, D.C. for SNBL, and R.S. for the SQUID measurements. S.G. and O.Z. performed the calculations and analysed the data. The manuscript was written by S.G., O.Z., T.F. and C.R., with input from all co-authors.

Competing financial interests

The authors declare no competing financial interests.

Methods

Crystal growth and synchrotron X-ray experiments. $MnSc_2S_4$ single crystals were grown with the chemical transport technique. Single-crystal synchrotron X-ray diffraction experiments were performed on the Swiss-Norwegian Beamline SNBL BM01 at the European Synchrotron Radiation Facility. Details for the crystal growth and the refinements are presented in the Supplementary Information.

Neutron diffuse scattering experiments. Neutron diffuse scattering experiments were performed on the high-flux time-of-flight spectrometer DNS at MLZ with a coaligned sample of approximately 30 mg. The pyrolytic graphite PG(002) monochromator together with a Be-filter were used to select the incoming neutron wavelength of 4.5 Å. To obtain the magnetic diffuse scattering signal, the intensities in the X spin-flip (SF) channel were measured, where the X direction is in the horizontal plane. The X-SF measurements at 50 K were subtracted as the background.

Spherical neutron polarimetry experiments. The polarized neutron diffraction experiments were performed on the cold neutron triple-axis spectrometer (TASP) with MuPAD at the spallation neutron source SINQ of the Paul Scherrer Institut and the thermal-neutron triple-axis spectrometer IN22 with CRYOPAD at the Institut Laue–Langevin. For the TASP measurements, the PG(002) monochromator and PG(002) analyser selected the neutron wavelength of 3.19 Å. The obtained matrices are presented in the Supplementary Information. For the IN22 measurements, the standard Heusler-Heusler configuration with a fixed neutron wavelength of 2.36 Å was used. A PG-filter was inserted before the sample.

Single-crystal neutron diffraction experiments. Neutron diffraction data sets were collected on the thermal-neutron diffractometer TriCS at SINQ of the Paul Scherrer Insitut. Incoming neutron wavelengths of 1.18 Å (Ge(311) monochromator) and 2.32 Å (PG monochromator) were used for the measurements. Under zero field, 135 and 62 reflections were collected at $T = 1.70$ and 1.35 K, respectively. 131, 50 and 56 reflections were collected at $H_{001} = 3.5$ T, $T = 1.38$, 1.62 and 1.85 K, respectively. Finally, 67 reflections were collected at $H_{111} = 3.5$ T, $T = 1.60$ K. Refinements were carried out using FULLPROF[42].

Mapping of the H–T phase diagram. The mapping of the H–T phase diagram was performed on TASP. A cryomagnet together with a dilution refrigerator was used. The PG(002) monochromator and PG(002) analyser selected the neutron wavelength of 4.22 Å. A PG-filter was installed in between the sample and the analyser. The crystal was mounted with the (HK0) plane horizontal. The intensity of the (0.75 0.75 0) reflection was carefully studied in cooling/warming processes under constant field and also in field-sweeping processes at constant temperatures. Reversibility across the phase boundary was used to separate the intrinsic phase transitions from domain effects.

Monte Carlo simulations. Monte Carlo simulations were performed using the ALPS package[43]. For the comparison with the DNS results, a $10 \times 10 \times 10$ superlattice was used. Calculations for the magnetic structure factor were averaged over 25,000 sweeps after 10,000 sweeps of thermalization.

Mean-field calculations. Interaction matrices were Fourier transformed to the reciprocal space and then diagonalized. Positions with the maximal eigenvalue produce the long-range-order $\boldsymbol{q}$-vectors at the mean-field approximation level. The dipolar interaction, when included, was cut beyond a distance of five unit cells.

Data availability. The data that support the plots within this paper and other findings of this study are available from the corresponding author upon reasonable request.

References

42. Rodrguez-Carvajal, J. Recent advances in magnetic structure determination by neutron powder diffraction. *Physica B* **192,** 55–69 (1993).
43. Bauer, B. *et al*. The ALPS project release 2.0: open source software for strongly correlated systems. *J. Stat. Mech. Theory Exp.* **2011,** P05001 (2011).